1 Introduction

"There are those who look at things the way they are,
and ask why...
I dream of things that never were,
and ask why not?"

Robert Kennedy

In the past 35 years, the scaling of metal-oxide-semiconductor field effect transistors (MOSFETs)[1] has powered the information technology revolution, enabling to double the device density, lowering cost per function and increasing the computational performance of integrated circuits every two to three years. As the device dimensions, i.e. the technology node, shrink below 100 nm, new physical phenomena start to interfere with traditional scaling laws[2]. The gate fails to control the charge carrier density at the semiconductor-dielectric interface (short-channel effect). Charge carriers interact increasingly more with the ionic lattice causing a velocity saturation. Leakage currents from the gate to the channel increase with ever thinner oxide thicknesses. Dielectric breakdown lowers the maximum voltage applicable across the gate oxide of the transistor.

To overcome such performance limitations and deliver the MOSFET performance increase, a combination of different strategies has been proposed: strain engineering, novel materials and novel device structures. Strain engineering has been the dominant method to deliver enhanced MOSFET performance during the last decade, offering a low-cost and low-risk solution and maintaining the traditional fabrication processes[3–8]. Strain has been a topic of interest in semiconductor research since 1950. Three years after the demonstration of the first point-contact transistor, John Bardeen and William Shockley developed the deformation potential theory to model the coupling between acoustic waves and electrons in solids[9]. With subsequent developments[10,11], such theory allowed to correctly predict physical effects like the increase in carrier velocity due to band warping, or the lower interband scattering due to the band degeneracy lifting[12]. The introduction of novel channel materials has also been explored as a method to increase the transistor performance. For example, III-V alloys offer electron mobilities higher than silicon up to 10 times, exceptionally high charge carrier velocities and outstanding frequency response. To improve the electrostatic control over the transistor channel with decreasing device dimensions, novel device structures have also been proposed. The industry is following a clear trend, moving away from planar device structures towards fins and nanowire channel devices with wrapped around gates. The effect of quantization is also expected to play a dominant role to obtain injection velocities significantly greater than bulk[13,14].

Elaborating and implementing strategies to permit the scaling of MOSFETs is not the only concern of the semiconductor industry. Since the power dissipated in electrical interconnects is rising above 80 % of the total energy used in the chip and the amount of heat that can be removed from each chip is saturating, there is a strong interest to develop new ideas around the distribution of information on and between integrated circuits. Integrating photonics on chip offers solutions to face these challenging power limits[15,16]. The integration of key photonic components, like p-i-n and avalanche photo-detectors or optical modulators, has been demonstrated using indirect bandgap semiconductors employed in traditional fabrication processes[17–20]. On the other end, the integration of a light source on silicon presents bigger challenges which can be tackled, once more, by using a combination of strain engineering, novel materials and nanostructured devices.

Strain engineering enabled to control and enhance the performance of III-V based optoelectronic devices. By modifying the energy bandgap, the valence and conduction band density of states, and the electronic wavefunction, strain made possible to tune the wavelength of emission[21], reduce the threshold current[22,23], suppress the Auger recombination[24] and intervalence band absorption processes[25], control the polarization[26], and improve

the overall efficiency of solid state lasers[27]. More recently, high anisotropic strain has been used to achieve a direct bandgap configuration in germanium[28–30], enabling the integration of a light source based on traditional group IV materials directly on silicon[31,32].

The nanowire geometry allows a direct integration of III-V materials on silicon[33–35] and offers a broader parameter space and opportunities to explore. Because of the small cross-section dimension of a nanowire, the mismatch of lattice constant and thermal expansion coefficient have a reduced impact on the crystal growth and quality. Increasing efforts in understanding the bottom-up growth of these structures[36–38] enabled unprecedented control over the morphology[39–44] and crystal structures[45,46] and alloy composition[47–50], leading to the synthesis of materials not available in bulk form, with novel optical properties[51,52]. The scope of nanowire research has also expanded beyond the above mentioned technological applications, enabling the realization of individually addressable entangled single photons sources[53–57], state-of-the-art photo-detectors[58–60] with single photon sensitivity[61], and found application in energy harvesting and photovoltaics[62–69].

Studying strain effects on novel III-V nanowires and nanostructured materials is therefore essential for the future information and communication technologies, having a strong influence on the future of MOSFET scaling and enabling on-chip optical communication. The impact of the discoveries generated by this research has a potentially broader range of influence, scientifically and technologically.

This thesis is devoted to studying uniaxial stress effects on GaAs nanowires. We chose this material as a model system for solid state light-emitting applications and focused our attention to experiments where a combination of nanoscale dimensions, novel materials and strain have a synergistic interplay. Recent theoretical calculations and experiments have highlighted that GaAs Zincblende nanowires exhibit enhanced mechanical properties and very high elastic range of deformation[70–73], which are a necessary requirement for enhanced effects on the band structure and on the optical and electronic properties. GaAs nanowires can also be grown with novel crystal structures, i.e. Wurtzite GaAs, not available in bulk or thin film form: the electronic bandstructure of this material is still highly controversial. We will show how uniaxial stress experiments can be used to disentangle and provide a clearer picture of the bandstructure.

The chapters 2 to 4 provide a concise but self-contained theoretical background, describing the concepts of mechanics and solid state physics that are needed to fully appreciate the experimental work. The chapters 5 to 8

are dedicated to the description of the instrumentation used, of the measurements performed, and to the physical interpretation and discussion of the results.

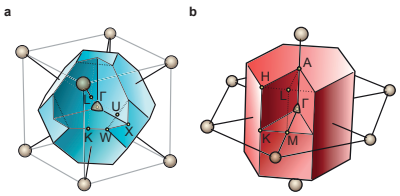

Chapter 2

We provide a general description of GaAs Zinc-blende and Wurtzite crystals. We describe their crystal structure, show the differences between their Brillouin zones, illustrate their bulk electronic band structure and dedicate special attention to the band states in proximity of the Γ-point. Finally we provide a description of the vibrational spectrum, showing the phonon dispersion relations and describing the corresponding geometries of atomic displacement.

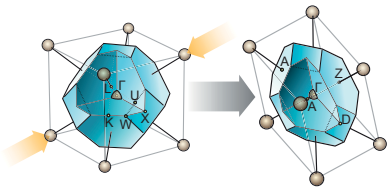

Chapter 3

The effects of strain on the band structure and lattice dynamics are treated here. We provide the basic definitions of stress, strain, compliance and stiffness tensors, derive the expression of the strain tensor upon uniaxial stress and decompose it into isotropic and deviatoric components. We describe the effect of strain on the conduction and valence band states using a $k \cdot p$ model, and on energy of the optical phonons using the deformation potential theory.

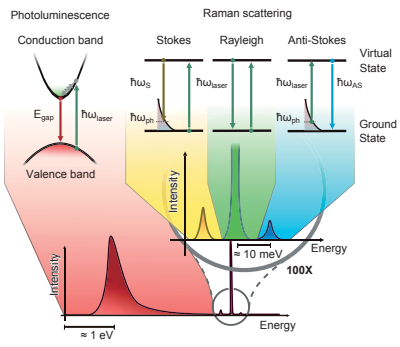

Chapter 4

We explain how strain effects can be observed experimentally using optical spectroscopy. We show how to model the photoluminescence lineshape and how to extract bandstructure parameters and other observables. We give a classical description of the Raman scattering process and show how to isolate the contribution of phonons with different symmetry using the polarization dependence of the Raman selection rules.

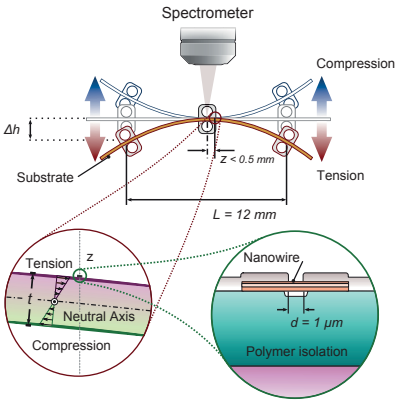

Chapter 5

The methods and the procedures used to perform the experiments are described here. We briefly summarize the methods used to grow Zincblende and Wurtzite nanowires, describe the steps used and highlight the challenges that were overcome to fabricate the nanowire strain devices. A brief description of the strain mechanism is given, followed by the analysis of the optical spectroscopy setup. We conclude the chapter with a summary of the nanoscale size effects that are expected for the particular nanowires employed in our experiment.

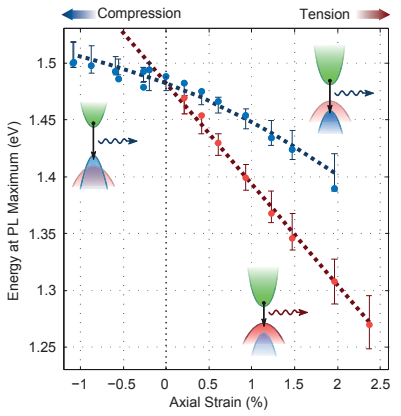

Chapter 6

The strain effects on Zincblende GaAs nanowires are studied: we demonstrate remarkable shifts of the energy bandgap by polarized photoluminescence measurements, explain how Raman spectroscopy can be used to fully characterize the strain tensor and the nanowire mechanical properties and provide a consistency check of our analysis by calculating the band edge deformation potentials of the nanowire. Finally we show the maximum strain and photoluminescence shift that can be obtained in such nanowire structures.

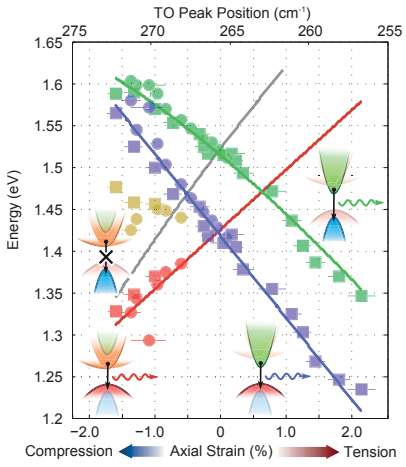

Chapter 7

The effect of strain on a Wurtzite GaAs nanowire is studied by photoluminescence and Raman spectroscopy: we show that uniaxial stress can cause a reversible quenching of the photoluminescence, which has been assigned to a direct-to-pseudodirect bandgap transition. By analyzing the results with a theoretical model, we could clarify the band structure of these crystals and resolve a controversial discussion about the energy and symmetry of the valence and conduction band states. Mechanical properties and phonon deformation potentials of the nanowire are also determined.

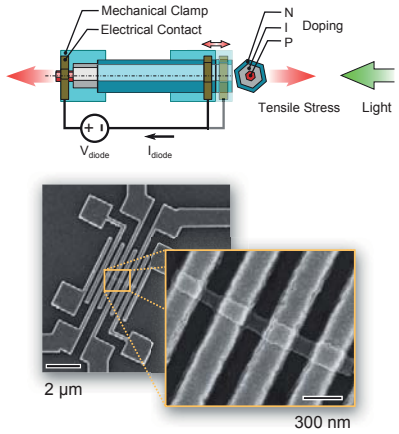

Chapter 8

We conclude this thesis summarizing our initial goals and the technical challenges that had to be overcome, providing an overview of the results of Zincblende and Wurtzite nanowires, and comparing them to each others. Finally we describe our vision of a new generation of devices which leverage the strain degree of freedom to achieve novel functionalities.

2

Electronic and Vibrational Properties of Zincblende and Wurtzite GaAs

This chapter provides the fundamentals concepts about the crystal structure and physical properties of Zincblende and Wurtzite crystals. We will describe the electronic bandstructure, the energy and atomic displacement of the optical phonons of these III-V crystals.

2.1 Crystal Structure

The structure of Zincblende and Wurtzite crystals can be defined using two different Bravais lattices and basis sets of atoms per unit cell. The Zincblende structure is constructed with the face centered cubic (FCC) lattice and a base set of two atoms, one of the group III, like Gallium (Ga), and one of the group V, like Arsenic (As). One lattice parameter a, i.e. the length of the edge of the cube, is needed to define the FCC lattice. The Wurtzite structure is created instead with a base set of four atoms associated to an hexagonal lattice, which is completely specified by the length of the edge of the hexagon a and the height of the parallelepiped c. The unit cells of Zincblende and Wurtzite crystals are represented in figure 2.1 and discussed with further detail in appendix A.

Even if appearing different at first sight, the two crystal structures have very much in common. In both structures every atom of group III is located

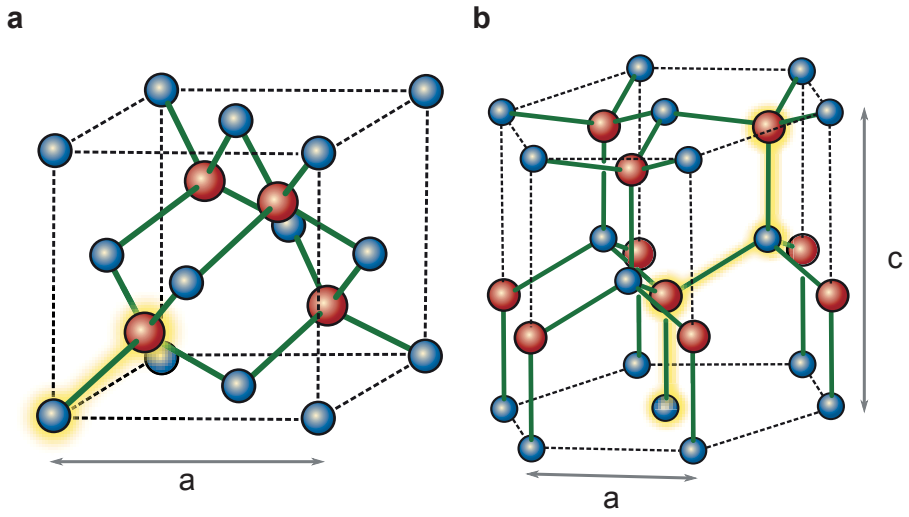

Figure 2.1: Unit cells of Zincblende (a) and Wurtzite (b) crystals. Atoms of the group III and V are shown in red and blue, respectively. The atoms constituting the base set are highlighted in yellow.

at the center of a regular tetrahedron, forming bonds with four atoms of the group V. The similarity between the two structures becomes even more evident if one rotates the Zincblende unit cell, orienting the z-axis parallel to the cubic [111] direction, and the x-axis and y-axis along [110] and [11$\bar{2}$]: both crystals are formed by stacking triangular lattices formed by the coordination tetrahedra on top of each others. Birmann highlighted that one can leverage such similarity and generate the Zincblende crystal shown in figure 2.2, using a basis containing six atoms and an hexagonal lattice, like in the Wurtzite case[74,75]. This definition highlights that the only difference between the two crystal structures resides on the sequence of stacking of tetrahedral planes, which is ABCABC for Zincblende and ABABAB for Wurtzite.

2.2 Electronic Band Structure

The Schrödinger equation that describes the dynamics of electrons and nuclei of Zincblende and Wurtzite semiconductors constitutes a very complex many-body problem and simplified solutions can be obtained only by using a number of assumptions. The valence electrons can be considered separately from the ionic lattice, constituted by the nuclei and the core electrons. Under the adiabatic approximation, the valence electrons experience only the potential generated by the static ionic lattice. With the mean field approximation, all valence electrons experience the same average potential

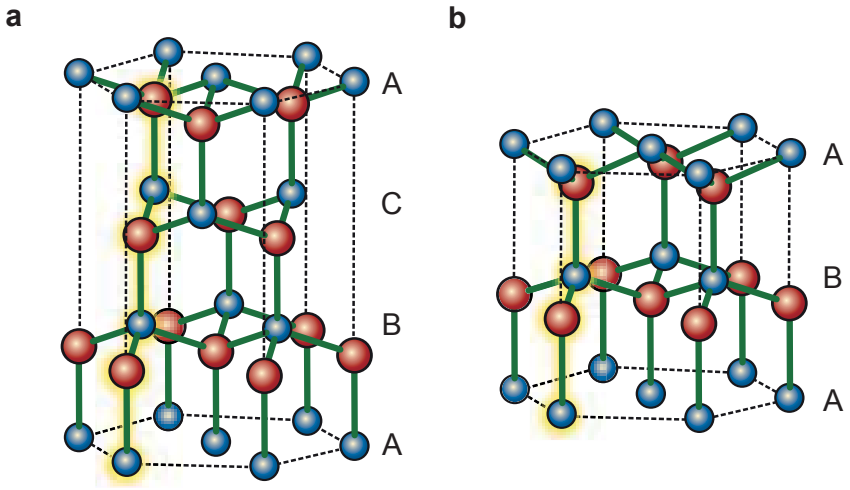

Figure 2.2: Defining the Zincblende crystal structure with the Birmann unit cell (a) highlights its similarity with the Wurtzite structure (b). In both structures, the base set is highlighted in yellow.

$V(\mathbf{r})$ generated by the ionic lattice and by the remaining valence electrons. Within these assumptions the Schrödinger equation for each single electron can be rewritten as[76]:

$$\mathscr{H}_{1e}\Phi_n(\mathbf{r}) = \left(\frac{p^2}{2m} + V(\mathbf{r})\right)\Phi_n(\mathbf{r}) = E_n\Phi_n(\mathbf{r})\,, \tag{2.1}$$

where $\mathscr{H}_{1e}$ is the one-electron Hamiltonian while $\Phi_n(r)$ and E_n denote the wave-function and energy of an electron in the eigenstate n, which can only accommodate two electrons with opposite spin.

The mean-field potential $V(\mathbf{r})$ will have the translational symmetry of the crystal itself and the electron wave-functions can be written as the sum of plane waves, with wave-vector $\mathbf{k}$, times an envelope function $\psi_{n\mathbf{k}}(\mathbf{r})$ that has the same periodicity as the crystal:

$$\Phi_n(\mathbf{r}) = \sum_{\mathbf{k}} \psi_{n\mathbf{k}}(\mathbf{r})\, e^{i\mathbf{k}\cdot\mathbf{r}}\,. \tag{2.2}$$

The periodic solutions and the energy spectrum E_n can be defined within a finite region of wave-vector space $\mathbf{k}$, with the symmetry of the reciprocal lattice, i.e. the Brillouin zone.

Figure 2.3 shows the reciprocal lattice and Brillouin zones for a FCC lattice (a) and for an hexagonal lattice (b): the high symmetry points at the surface are marked with capital latin letters, while the center is indicated in both structures with the greek letter Γ. Using these definitions, it is possible

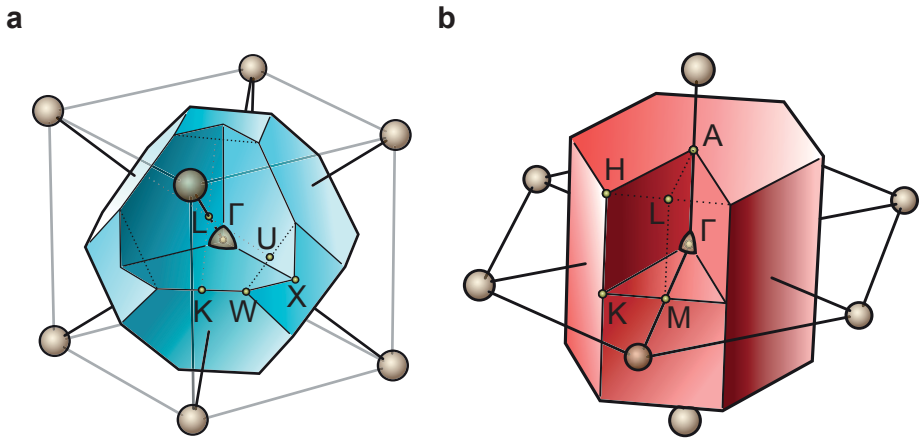

Figure 2.3: Brilluoin zones for (a) Zincblende and (b) Wurtzite crystals.

to represent the dependence of $E_n(\mathbf{k})$ on the wave-vector along lines that connect high symmetry points within the Brillouin zone.

2.2.1 Band Structure of Zincblende GaAs

Density Functional Theory (DFT) can be used to calculate the energy-momentum relation of Zincblende GaAs[77]. The energy values along the high symmetry directions are shown in figure 2.4a. The energy levels that determine optical and electrical properties of the material are highlighted with a dashed line and magnified in a sketch in figure 2.3b.

The valence band states, i.e. the highest occupied electronic states, are characterized by quadratic relation between energy and wave-vector and one can describe them as free charged particle with modified "effective" mass. The two valence bands with the highest energy are degenerate at the Γ-point but have a different energy wave-vector relation: the heavy hole band is associated to an effective mass m_{hh} that, depending on the direction of the wave-vector, ranges between $0.33\,m_e$ and $0.81\,m_e$ [*]. The light hole band instead has overall a smaller effective mass m_{lh}, which ranges between $0.080\,m_e$ and $0.094\,m_e$, depending on the wave-vector direction[78]. A third band, called split-off hole, has an almost isotropic effective mass $m_{\mathrm{so}} \approx 0.182\,m_e$ and is found at lower energy compared to the heavy hole and light hole states. This energy difference (340 meV) is a manifestation of the spin-orbit interaction, i.e. the interaction of the spin of the electron with its own angular momentum. The conduction band states, formed by the lowest unoccupied electronic states, also have a minimum energy at the Γ-point and parabolic energy wave-vector relation, with $m_{\mathrm{cb}} \approx 0.066\,m_e$. The

[*] m_e is the mass of a free electron.